Nano World Journal

https://doi.org/10.17756/nwj.2023-s3-132

Research Article

Open Access

Improved Mechanical and Tribological Characteristics in AA5052-nano Silicon Carbide Metal Matrix Nanocomposites by Ultrasonic Cavitation Casting

Barun Haldar[1*], S. Vinodh[2], B. Deepa[3], Mayank Choubey[4], S. Kiruba[5], Tenepalli Jaisai[6] and P. Satishkumar[7]

[1]*Department of Mechanical and Industrial Engineering, College of Engineering, Imam Mohammad Ibn Saud Islamic University, Riyadh, Saudi Arabia*

[2]*Department of Mechanical Engineering, Sri Eshwar College of Engineering, Coimbatore, Tamil Nadu India*

[3]*Department of Science and Humanities, Karpagam Academy of Higher Education, Coimbatore, Tamil Nadu, India*

[4]*S.G.T. University, Gurgaon, Haryana, India*

[5]*Department of Physics, St. Joseph's College of Engineering, Chennai, Tamil Nadu, India*

[6]*School of Construction, NICMAR University, Pune, Maharashtra, India*

[7]*Department of Mechanical Engineering, Rathinam Technical Campus, Coimbatore, Tamil Nadu, India*

[*]Correspondence to:
Barun Haldar
Department of Mechanical and Industrial Engineering,
College of Engineering,
Imam Mohammad Ibn Saud Islamic University,
Riyadh, Saudi Arabia.
E-mail: maalmeshaal@imamu.edu.sa

Received: July 31, 2023
Accepted: October 30, 2023
Published: November 01, 2023

Citation: Haldar B, Vinodh S, Deepa B, Choubey M, Kiruba S, et al. 2023. Improved Mechanical and Tribological Characteristics in AA5052-nano Silicon Carbide Metal Matrix Nanocomposites by Ultrasonic Cavitation Casting. *NanoWorld J* 9(S3): S745-S751.

Copyright: © 2023 Haldar et al. This is an Open Access article distributed under the terms of the Creative Commons Attribution 4.0 International License (CCBY) (http://creativecommons.org/licenses/by/4.0/) which permits commercial use, including reproduction, adaptation, and distribution of the article provided the original author and source are credited.

Published by United Scientific Group

Abstract

Ultrasonic cavitation was used to cast AA5052-nano silicon carbide (nSiC) metal matrix nanocomposites (MMNCs) for this research. With the addition of nano silicon carbide particles ($nSiC_p$) to the AA5052 matrix, the material's hardness, tensile strength, and impact resistance were all considerably improved. The addition of $nSiC_p$ to AA5052 increased its strength and hardness without decreasing its elasticity or impact absorption. The AA5052 composite containing 2.4% volume of $nSiC_p$ showed the greatest improvement in strength, at almost 124% greater than the standard alloy. The composite with 3% volume of $nSiC_p$ exhibited the highest hardness, which was another important discovery. After incorporating 2.4% $nSiC_p$, the composite lost some of its pliability and impact resistance as a result of the particles clumping together. Wear resistance qualities of AA5052-nSiC composites were found to be superior to those of monolithic AA5052s in dry sliding wear pin-on-disc tests.

Keywords

Cavitation, Nanocomposites, Ultrasonic, Wear, Elasticity, Hardness

Introduction

MMNCs have advanced significantly in several areas of engineering in recent years [1]. Unlike traditional metal matrix composites, MMNCs do not suffer from the same drawbacks, such as low ductility, poor fracture toughness, and difficulty in being machined. Multinational corporations have an outsized interest in the athletic, maritime, automotive, and military industries. However, their extensive application is hampered by the high production cost of MMNCs.

The increased surface area of nanoparticles causes nanosized powders to agglomerate more readily than larger particles. As a result, conventional methods have a very hard time achieving a uniform mixture of the nanoparticles in metal matrix. The foregoing issues are motivating the development of novel processing techniques for the fabrication of MMNCs featuring homogenous nanoparticle dispersions [2]. Mechanical stirring, electromechanical stirring, and ultrasonic cavitation-assisted stirring are just a few of the mixing strategies that have been used to synthesize the MMNCs. Mechanical stirring creates a vortex in a melt that already has reinforcements by using a rotating impeller [3, 4]. The problem with mechanical stirring is that the particles rise to the top of the melt as soon as the swirling stops. Ultrasonic cavitation-assisted casting, in which nanoparticles are dispersed in a liquid melt, is an innovative and highly promising method [5].

Past applications of ultrasonic cavitation effects include melt degassing, grain refinement, and deagglomeration of nanoparticles. When ultrasonic aided casting is used to disperse nanoparticles in liquid melts, high-intensity ultrasonic waves present the liquid, leading to ultrasonic nonlinear phenomena such transient cavitation and acoustic streaming. Microstructure refinement, liquid degassing, and particle homogenous dispersion are all results of ultrasonic nonlinear effects.

High-intensity ultrasonic cavitations can cause implosive effects that can break up agglomerated nanoparticles and evenly disperse them in metal melts. In contrast to mechanical mixing or electromechanical mixing, cavitation bubbles generate localized energy levels that are many times greater. The wettability of the melt to the nano-reinforcements is increased, and the nanoparticles are uniformly dispersed throughout the melt, thanks to ultrasonic nonlinear effects [6].

When it comes to the weight of structural components, industries including the automotive, aerospace, and transportation sectors favor metal matrix composites made from aluminum (Al). SiC is one of the lightest and toughest reinforcing materials, with a Mohs hardness of 9.497. SiC's bonding capabilities with AA5052s are exceptional, especially when compared to those of other ceramic reinforcements [7]. Therefore, by incorporating SiC nanoparticles, which are both high modulus and highly hard, into an Al matrix, a stiff and strong nanocomposite can be created.

Both A356/nSiC and magnesium/nSiC have been the subject of extensive research into the use of ultrasonic cavitation in nanomanufacturing. SiC nanoparticles in Al melts have been modelled and deagglomerated, according to published research [8]. Hybrid composites have been synthesized using an ultrasonic cavitation process, according to the published literature [9]. Al-SiC composites were created using powder metallurgy and mechanical alloying techniques. Research on the effects of impacts and wear on conventional composites made of Al/SiC was published [10].

From the above, it is apparent that just a little amount of effort was put into preparing and characterizing Al/nSiC$_p$ MMNCs utilizing an ultrasonic cavitation technique. In this work, an ultrasonic cavitation technique was used to produce high-performance lightweight bulk Al/nSiC MMNCs and investigate their properties.

Materials and Method

AA5052 possesses low density in addition to its favorable formability and corrosion resistance qualities. In this research, ceramic nanoparticles made of SiC were used as reinforcement (average size 50 nm). Adding micro SiC to AA5052 has the potential to boost its hardness and other mechanical qualities without significantly increasing the component's overall weight. Since Al and SiC have such a large thermal expansion coefficient difference, the dislocation density is amplified [11]. The high dislocation density is mostly responsible for the enhanced tensile strength. Since SiC has a density similar to that of Al, no separation will occur during manufacturing. Table 1 shows some typical matrix and reinforcement properties.

Table 1: Chemical composition of AA5052.

Si	0.25%
Mg	2.2%
Cu	0.0%
Fe	0.40%
Mn	0.10%
Zn	0.10%
Cr	0.15%
Al	Balance

The nanocomposites were cast in a crucible made of stainless steel (SS 310 grade) that measured 165 mm in length and 65 mm in diameter. The 2 kHz electrical signal produced by the 2-kW ultrasonic generator is generated by inverting the 230 V line current. A piezoelectric transducer converts the electrical signal's high frequency into mechanical vibrational energy at 20,000 Hz. High-frequency vibrations are linked to the booster horn and sent into the melt, where they cause strong cavitation. Three distinct input amplitudes are available to the generator, allowing for three distinct melt processing output amplitudes to be obtained.

The titanium alloy horn was used in melt processing. The dipping portion of the titanium horn has a diameter of 20 mm and a length of 185 mm, while the top portion, which is connected to the transducer, has a diameter of 35 mm and a length of 85 mm. In order to get the necessary frequencies into the melt, a transducer, booster, and horn are all tuned equipment that are employed. A thermocouple was used to track the melting process's temperature. Ultrasonic horn movement up and down during sonication is partially regulated using compressed air for cooling purposes (ultrasonic processing). Casting Al requires a constant flow of argon gas over the surface of the melt to prevent oxidation.

Different volume percentages of nSiC$_p$ were used in tests to investigate the ultrasonic nonlinear effects on processing molten materials. Choking the furnace at 680 °C for around 10 min allowed 800 g of metal to melt.

After the alloy melt was homogenized through mechanical stirring, nSiC$_p$ were added gently from above while continuing to agitate the mixture. The Al melt is mechanically stirred at 700 rpm to pre-mix the nanoparticles and reduce the sonication duration.

After the first mixing has been done mechanically, the ultrasonic probe is lowered into the liquid and the ultrasonic wave generator is switched on to further disperse the substance. When ultrasonic waves are applied to molten Al, they create vast quantities of cavitation bubbles within the material because their intensity (energy) is greater than the bonding energy of the liquid. When cavitation bubbles implode during a high-pressure cycle, they scatter the nanoparticles around them uniformly in all directions. Therefore, effective ultrasonic processing considerably reduces nanoparticle agglomeration tendencies. For the melt processing, 45 min of sonication time was employed in conjunction with intermittent vibrating mode [12].

An ultrasonic generator with a 2-kW power rating and a 20 mm horn diameter was used in this study. Ultrasound decibels are calculated by dividing the horn's total power output by its effective radiating area. With an ultrasonic power density of 80 - 100 W/cm^2 cavitation can be induced in metal melts [9, 13]. Due to the high levels of ultrasonic energy generated, cavitation is effectively stimulated, and particles are disseminated uniformly throughout the alloy melt. Melted metal can't flow as easily into a warmed steel die when $nSiC_p$ are added since the mixture's viscosity increases considerably. Sonication followed by 850 °C of heating was performed on the material before it was inserted into the die. In this study, we use ultrasonic cavitation-assisted casting to create Al/$nSiC_p$ MMNCs with $nSiC_p$ loadings of 0%, 0.6, 1.2%, 1.8%, 2.4%, and 3%.

Specimens of the plain alloy and MMNCs are reduced to a thickness of around 300 µm using wire electric discharge machine. More than an hour is spent hand-polishing each specimen with emery sheets. After hand polishing, the samples are determined to have a thickness of roughly 100 mm. Mechanical polishing produces 20-mm-thick foils with a surface smoothness of 50 nm from the manually polished samples. Thick samples are ground down using dimple grinding or ion milling devices. The discs are punched with a disc punch and then cut with an ultrasonic disc cutter, both of which are 3 mm diameters.

All AA5052-nSiC composites are subjected to brinell hardness testing in accordance with ASTM E10 using 10 mm steel balls and 500 kgf stress applied for a specified dwell duration of 20 sec. Five separate brinell hardness tests are averaged together to provide a single BHN result.

To assess the tensile behavior of the MMNC compositions, four tensile test specimens were prepared according to the ASTM E8 standard. Tensile testing was performed using INSTRON's universal testing machine. The elongation of the sample is found by comparing the initial and final gauge lengths. Each MMNC composition's universal tensile strength (UTS) and elongation percentage are determined. The tensile characteristics are calculated as the mean of the results from four separate tensile tests.

According to the ASTM E23 standard, four Charpy impact test specimens are developed to examine the nanocomposites' impact behavior. Charpy impact tests were conducted on AA5052-nSiC composites using a YAMA impact testing machine. The average of the results from four separate impact tests is used to determine the impact attributes Table 2.

The wear behavior of plain alloy and nanocomposites was studied by fabricating three pin-on-disc wear test specimens according to ASTM G-99 standards and pins were tested using pin-on-disc wear testing equipment. Machine wear, frictional force, and frictional coefficient may all be measured with the help of the included WINDCOM program. The data from three separate pin-on-disc wear tests to determine the wear characteristics were averaged.

Results and Discussion

When reinforcement was added to a metal matrix, the properties of the matrix material undergo a profound transformation. When $nSiC_p$ are present, the strain in MMNCs is not distributed uniformly, even when the load is supplied uniformly. The dissimilarity in coefficient of thermal expansion (CTE) and elastic modulus between AA5052 and SiC results in residual stresses within the nanocomposite. This occurrence contributes to an increase in dislocation density in nanocomposites when compared to simpler alloys.

The disparity in CTE between the Al alloy and the $nSiC_p$ induces a strain mismatch in the nanoparticles due to temperature fluctuations during the solidification process of the composite material [14],

$$\varepsilon_{CTE} = \left(C_m - C_p\right)\Delta T = \Delta C \Delta T \quad (1)$$

More dislocations can be seen in the photos, clustered around the nanoparticles. The cause is an upsurge in residual stresses along the matrix-reinforcement contact. Over a 200 nm^2 area, dislocations may be monitored in both the as-cast alloy and the nanocomposites. More dislocations may be seen in the nanocomposites than in the monolithic alloy in the chosen region.

Hard nanoparticles will limit the mismatch in deformation between MMNCs. As a result, the nanoparticles' surfaces will develop a substantial quantity of loop-like structure to counteract the deformation. This causes the nanocomposite structure to acquire heat residual stresses. Large numbers of dislocations are created in the manufactured composites as a result of thermal residual stresses. The created dislocations will stack up and interact with one another, slowing the dislocations down. Therefore, the nanocomposite's strength rises even with a negligible percentage of nanoparticles by volume [9].

Incorporating hard $nSiC_p$ into an MMNC matrix makes it more difficult for the matrix to deform under constant compressive pressure. It causes a buildup of dislocations at the nanoparticles' surface, which degrades their quality. Due to an increase of dislocations in the MMNC, the yield strength of the matrix is maintained. The volume proportion and particle size of SiC influence the strength of the nanocomposite by affecting the number of dislocations and the size of the matrix grains, respectively. The percentage of particle volume occupied

Table 2: Properties of AA5052 and $nSiC_p$.

Material	Modulus of elasticity (GPa)	Melting point (°C)	CTE K^{-1}	Thermal conductivity (W/mK)	Density (g/cm^3)
AA5052	69.3	607	2.38 x 10^{-5}	138	2.68
$nSiC_p$	423	2830	3.2 x 10^{-6}	35	3.16

by dislocations grows as particle size grows [15]. Spot spectra obtained using energy dispersive X-ray (EDX) spectroscopy are displayed in figure 1 for the AA5052/SiC_p nanocomposite. Si, Al, C, and B were shown prominent peaks because the EDX beam was actually focused over a wider spectrum. This spectrum shows that the nanocomposite was successfully protected from oxygen during manufacturing because no oxygen was detected. This was because argon gas was constantly being pumped into the system.

The hardness behavior of AA5052-nSiC composites as a function of nSiC content is shown in figure 2. As the percentage of particles in nanocomposites rises, so does their strength. The hardness of MMNC reinforced with 1% $nSiC_p$ is 118 BHN, which is much higher than the hardness of plain AA5052 alloy.

The enhanced hardness of the nanocomposites was attributed to the addition of $nSiC_p$, their exceptional bond with Al, and the uniform integration of SiC into the Al matrix through ultrasonication. Because the inserted $nSiC_p$ block dislocation motion, the hardness is increased. Because dislocation motion is impeded by the reinforcement, nanocomposites became harder as their reinforcement content approached its maximum. The enhanced hardness of the nanocomposites is due in part to the fact that the particle concentration around the indentation increases as the indenter is lowered during the hardness test.

Figure 3 shows how the tension behavior of Al alloy/SiC MMNCs is modified by the presence of $nSiC_p$. Figure 3 demonstrates that, up to a volume of 2 vol.%, the UTS of a material increases as the percentage of micro SiC particles increase, but afterwards decreases. The tensile strength is improved due to the interaction of the ultrafine SiC particles with the dislocations. The UTS value goes down for the $nSiC_p$, 3 vol.% composition specimen. This is because the MMNCs, notable porosity content and enhanced agglomeration of particles may counteract the aforementioned favorable effect of adding $nSiC_p$.

UTS averages 132MPa for unmodified AA5052 alloy and 294MPa for AA5052/2.4 vol.% SiC_p MMNC. When compared to a plain alloy, MMNC has a UTS increase of about 130%. This material's strong strength-to-weight ratio and relatively high ductility make it suitable for a wide range of prospective structural applications.

In figure 4, the reinforcing $nSiC_p$ affects the AA5052-nSiC MMNC's percent elongation to fracture was monitored. Nanocomposites are found to retain nearly all of their ductility (as measured by percent elongation) up to 2.4 vol.% of SiC. Even though the SiC particles seemed to be micro-clusters in places, the material maintained its ductility because the clusters were still separated by nanoparticles. Uniformly disseminated SiC counteracts the detrimental effect of micro-clusters by reinforcing and reefing the grain. In addition, the ductility of nanocomposites is much better than that of traditional composites. Above a particle volume percentage of 2.4, ductility in the aforementioned composites drastically reduces because of early void formation and high porosity content.

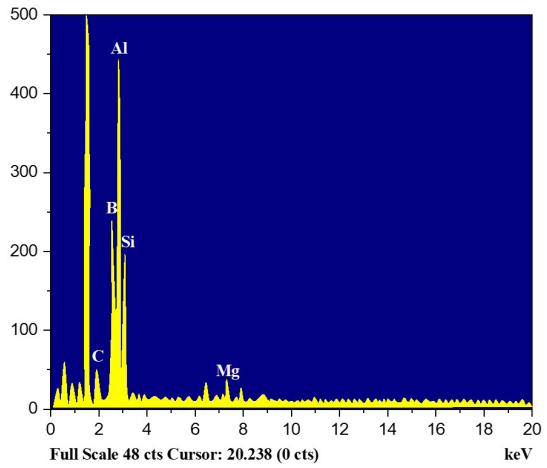


Figure 1: EDX on AA5052/3 vol.% $nSiC_p$ MMNC.

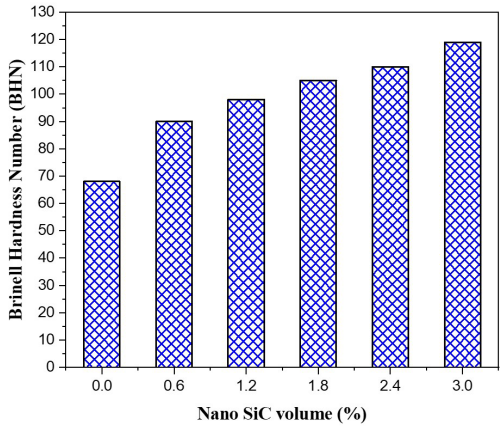


Figure 2: Impact of $nSiC_p$ on hardness.

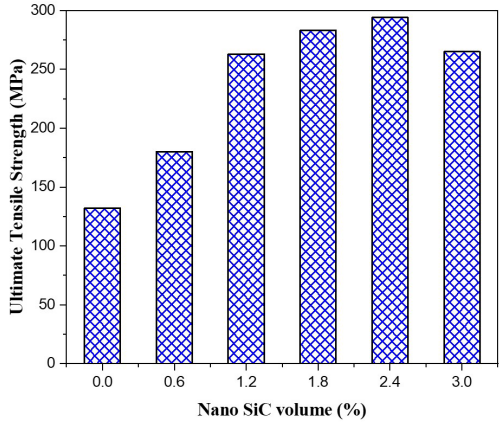


Figure 3: Impact of $nSiC_p$ reinforcement on tensile strength.

Figure 5 displays the impact energy of AA5052-nSiC composites as a function of nSiC reinforcement. The impact energy is slightly diminished up to a volume content of 2.4% nSiC in a metal matrix, and then it drops down dramatically after that. This is because $nSiC_p$ decohere and fail. Impact energy absorption can also be affected by the presence of defects in the nanocomposite.

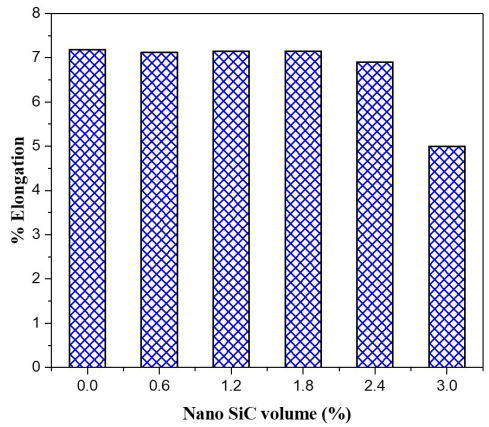


Figure 4: Impact of $nSiC_p$ reinforcement on percentage of elongation to fracture.

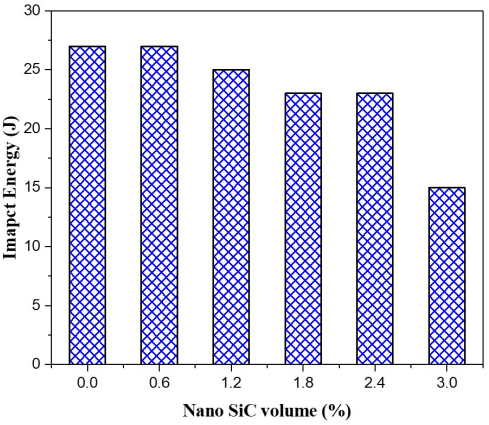


Figure 5: Impact of $nSiC_p$ reinforcement on impact energy.

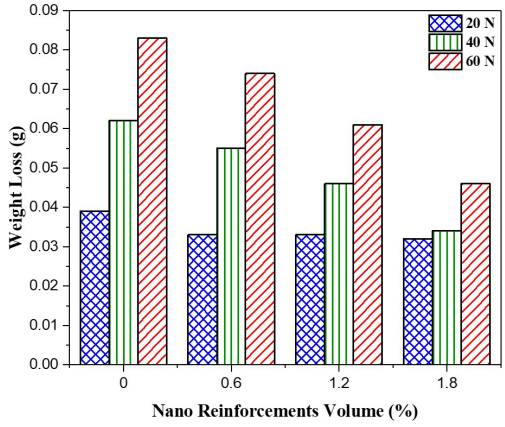


Figure 6: Impact of $nSiC_p$ reinforcement on wear.

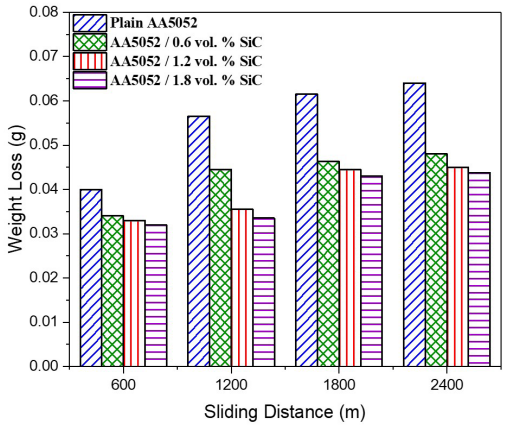


Figure 7: Wear vs Sliding distance.

Pin wear is quantified by a drop-in weight. Parameters such as track diameter (450 mm), rotational speed (500 rpm), sliding distance (600 m), and sliding velocity (1.5 m/s) are held constant throughout the studies.

Weight loss in the pins can be reduced by increasing the $nSiC_p$ content, as shown in figure 6. As the load is increased, the pins lose less mass across the board. In addition, AA5052 reinforced with 1.8 vol.% of $nSiC_p$ exhibits the least amount of weight loss in this investigation. This is because extremely hard $nSiC_p$ were dispersed throughout the material and used as load bearing elements, increasing its hardness. Wear resistance is enhanced by increasing the material's hardness.

Figure 6 further shows that plain AA5052 had much inferior wear resistance qualities than the MMNCs. The AA5052 has a weight loss of 0.062 g under a standard load of 40 N, while the AA5052/1.8 vol.% $nSiC_p$ has a weight loss of 0.034 g. Weight savings of almost 136% when using MMNC instead of standard AA5052 is impressive and useful in many wear-resistant contexts.

Figure 7 displays the correlation between the sliding distance and the weight reduction for both plain AA5052 and MMNCs. Sliding at a speed of 1.5 m/s and under a normal stress of 20 N, the trials are conducted. From the graph, it's clear that longer sliding distances lead to more pin wear. Compared to nanocomposites, it rises dramatically for unmodified AA5052. Increasing the rotational speed is a significant contributor to accelerating the wear process. The Al matrix ages prematurely and softens as a result of the increased heat created at the contact point between the Al pin and the disc as the rotational speed increases. Matrix weakening caused by high heat output increases wear rate.

Figure 8 displays the plain AA5052 and MMNCs' weight loss of pins as a function of sliding velocity. The aforementioned tests are conducted with 20 N delivered at sliding speeds of 1.5 m/s, 2 m/s, and 2.5 m/s. The plotted graph illustrates a direct correlation between the increase in sliding speed and the corresponding rise in weight loss for both MMNCs and monolithic alloys. The accompanying image visually demonstrates that among the nanocomposites enhanced with 1.8 vol.% $nSiC_p$, the weight loss was minimized.

Frictional coefficients as a function of normal load are depicted in figure 9 to figure 11 for both unreinforced alloys and MMNCs. Graphs are displayed for sliding rates of 1.5 m/s, 2 m/s, and 2.5 m/s across a fixed distance of 2400 m. The average frictional coefficient decreases with increasing normal load and $nSiC_p$ concentration. After sliding for around 1800 m, the

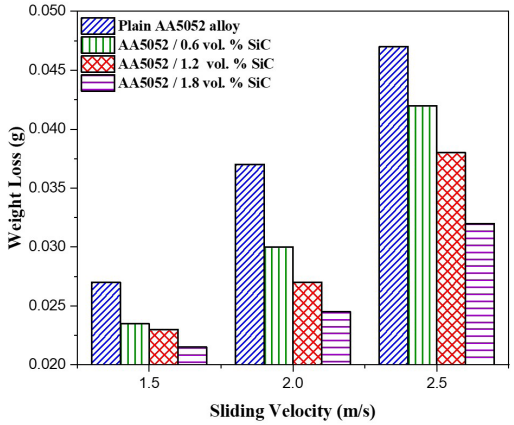


Figure 8: Wear vs Sliding velocity.

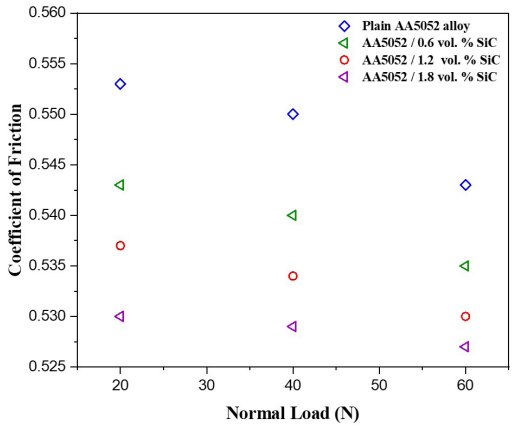


Figure 9: CoF vs Load at 1.5 m/s.

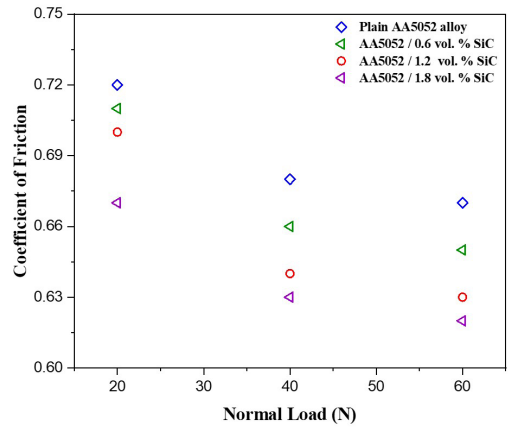


Figure 10: CoF vs Load at 2 m/s.

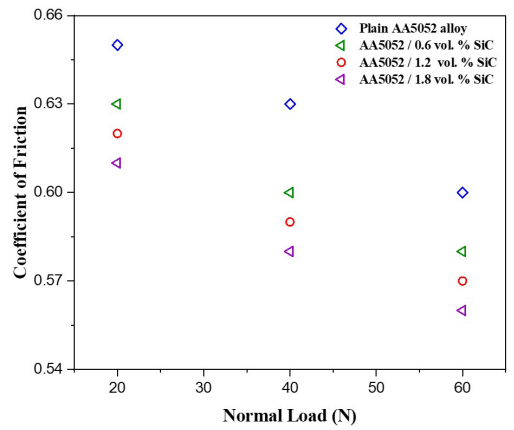


Figure 11: CoF vs Load at 2.5 m/s.

friction coefficient stabilizes after initially being quite high. Higher frictional coefficients under lower normal loads can be described as follows: because of less initial contact between asperities, abrasive action is greater, and so is the coefficient of friction (CoF). The ploughing action and the CoF are both reduced when the normal load increases because the contact surfaces become more homogeneous.

When force is applied, the material is prevented from relocating due to the incorporation of $nSiC_p$. Hard counter faces show less ploughing than the matrix alloy does. The pin's worn surface shows clear shearing and ploughing marks, lending credence to the aforementioned notion. When an Al pin slide over a steel disc, similar results are seen. In contrast to normal AA5052s, surface shearing is significantly more intense in the case of MMNCs.

Conclusion

Successful development of AA5052/$nSiC_p$ MMNCs using ultrasonic cavitation-assisted casting approach (average particle size 50 nm). By increasing the $nSiC_p$ volume fraction in AA5052, the material's BHN and UTS were significantly improved, but the failure strain and impact strength were nearly unaffected. The tensile strength of AA5052/2.4 vol.% $nSiC_p$ MMNC is exceptional. When compared to a monolithically cast alloy, this system's UTS improvement is greater than 124%. The AA5052/3% $nSiC_p$ system had the highest BHN of any tested system. Up until around 2.4 vol.% of $nSiC_p$ is added, the nanocomposite's ductility and impact strength are almost completely preserved; after that point, the value rapidly decreases due to increased agglomeration of the particles. Nanocomposite reinforcement with 2.4 vol.% $nSiC_p$ improved ductility and impact strength retention over plain Al alloy by 95% and 89%, respectively. Wear tests on both monolithic and Al alloy-MMNC samples showed that the latter had superior wear resistance. As the volume fraction of reinforcement in Al alloy rises, the material's wear resistance improves. The wear rate of Al alloys and Al nanocomposites rises with the velocities, distances, and loads involved in sliding. Nanocomposites have been found to have a slower rate of wear rate increase than ordinary alloys. Increases in reinforcement volume percentage and normal load led to a decrease in the CoF.

Acknowledgements

None.

Conflict of Interest

None.

References

1. Bodaghi M, Dehghani K. 2017. Friction stir welding of AA5052: the effects of SiC nano-particles addition. *Int J Adv Manuf Technol* 88: 2651-2660. https://doi.org/10.1007/s00170-016-8959-8
2. Dinesh Kumar D, Balamurugan A, Suresh KC, Suresh Kumar R, Jayanthi N, et al. 2023. Study of microstructure and wear resistance of AA5052/B_4C nanocomposites as a function of volume fraction reinforcement to particle size ratio by ANN. *J Chem* 2023: 2554098. https://doi.org/10.1155/2023/2554098
3. Faraji M, Karimi S, Esmailzadeh M, Pezzato L. 2023. Investigation of the microstructure and corrosion behaviors of composite hard-faced layers on Al5052 using SiC and TiB_2 in 3.5% NaCl and 0.5 M H_2SO_4 solutions. *J Mater Eng Perform* 32(21): 9711-9724. https://doi.org/10.1007/s11665-023-07807-7
4. Faraji M, Karimi S, Esmailzadeh M, Pezzato L, Calliari I, et al. 2022. The electrochemical and microstructure effects of TiB_2 and SiC addition to AA5052/Al_2O_3 surface composite coatings in 0.5 M H_2SO_4 solution. *J Bio Tribo Corros* 8(4): 117. https://doi.org/10.1007/s40735-022-00716-7
5. Gara L, Zou Q. 2013. Friction and wear characteristics of oil-based ZnO nanofluids. *Tribol Trans* 56(2): 236-244. https://doi.org/10.1080/10402004.2012.740148
6. Harichandran R, Selvakumar N. 2016. Effect of h-BN solid nano lubricant on the dry sliding wear behaviour of Al-B_4C nanocomposites. *Arch Mater Sci Eng* 77(1): 5-11.
7. Srinivasan R, Karunakaran S, Hariprabhu M, Arunbharathi R, Suresh S, et al. 2023. Investigation on the mechanical properties of powder metallurgy-manufactured AA7178/$ZrSiO_4$ nanocomposites. *Adv Mater Sci Eng* 2023: 3085478. https://doi.org/10.1155/2023/3085478
8. Kim S, Hong J, Joo Y, Kang M. 2022. Synergistic effect of SiC nano-reinforcement and vibrator assistance in micro-friction stir welding of dissimilar AA5052-H32/AA6061-T6. *J Manuf Process* 82: 860-869. https://doi.org/10.1016/j.jmapro.2022.08.023
9. Srinivas PS, Babu PR, Balakrishna B. 2020. Material characterization and optimization of CNT-reinforced aluminum (AA7075) functionally graded material processed by ultrasonic cavitation. *Funct Compos Struct* 2(4): 045002. https://doi.org/10.1088/2631-6331/abb196
10. Paul T, Joshi R, Exime A, Edward W, Zhang C, et al. 2022. Role of ultrasonic treatment on microstructure, multiscale mechanical, and tribological behavior of 2D tungsten disulfide reinforced aluminum composites. *Adv Eng Mater* 24(12): 2200543. https://doi.org/10.1002/adem.202200543
11. Paul T, Zhang C, Denis N, Boesl B, Agarwal A. 2021. Role of ultrasonic treatment on microstructure, mechanical and tribological behavior of 2D boron nitride reinforced aluminum composites. *Mater Sci Eng A* 809: 140970. https://doi.org/10.1016/j.msea.2021.140970
12. Sarvaiya J, Singh D. 2023. Influence of hybrid pin profile on enhancing microstructure and mechanical properties of AA5052/SiC surface composites fabricated via friction stir processing. *Can Metall Q* 62(3): 426-439. https://doi.org/10.1080/00084433.2022.2114124
13. Singh D, Sarvaiya J. 2023. Development of AA5052/TiO2/SiC hybrid surface composites using upward material flow through multipass friction stir processing. *J Adhes Sci Technol* 37(23): 3335-3357. https://doi.org/10.1080/01694243.2023.2202952
14. Ping W, Yongzhen L. 2021. Preparation and tribological properties of covalent organic framework nanomaterials. *Tribology* 42(1): 123-130.
15. Kumar HP, Xavior MA. 2017. Assessment of mechanical and tribological properties of Al 2024-SiC-graphene hybrid composites. *Procedia Eng* 174: 992-999. https://doi.org/10.1016/j.proeng.2017.01.251